Collisional rates based on the first potential energy surface of the NeH+ –He system

Cheikh Bop, K. Hammami, N. P. Faye

Monthly Notices of the ROYAL ASTRONOMICAL SOCIETY

MNRAS **470,** 2911–2917 (2017) doi:10.1093/mnras/stx1369
Advance Access publication 2017 June 3

Collisional rates based on the first potential energy surface of the NeH^+ −He system

Cheikh T. Bop,[1]★ K. Hammami[2] and N. A. B. Faye[1]

[1]*Laboratory of Atoms Lasers, Departement of Physics, Faculty of Sciences and Techniques, University Cheikh Anta Diop, Dakar 5005, Senegal*
[2]*Laboratory of Atomic Molecular Spectroscopy and Applications, Departement of Physics, Faculty of Sciences, University Tunis El Manar, Campus Universities, 1060 Tunis, Tunisia*

Accepted 2017 May 31. Received 2017 May 26; in original form 2017 May 3

ABSTRACT

The potential energy surface is computed at the explicitly correlated coupled cluster with simple, second and perturbative triple excitation method (CCSD(T)–F12) in connection with the augmented–correlation consistent–polarized valence triple zeta (aug–cc–pVTZ) Gaussian basis set for the NeH^+ −He system. The calculations were performed by first taking into account the vibration of the molecule and then averaging the so-obtained three-dimensional potential. From this average interaction potential, cross-sections among the 11 first rotational levels of NeH^+ induced by collision with He are calculated for energies up to 4000 cm^{-1} using the quantum mechanical close coupling (CC) approach. Collisional rate coefficients are obtained by thermally averaging these cross-sections at low temperature ($T \leq 300$ K). The propensity rules of the rotational transitions obtained in this paper are discussed and compared with those of HeH^+ and ArH^+ in collision with electron. This work may be helpful for the eventual investigations, both theoretical and experimental, focused to detect the key cationic noble gas hydride NeH^+ in the interstellar and circumstellar media as well as in laboratory experiments.

Key words: molecular data – molecular processes – ISM: abundances – ISM: molecules.

1 INTRODUCTION

Hydrogen and helium are the most abundant interstellar components and originate from primordial nucleosynthesis (Zygelman, Stancil & Dalgarno 1998; Ferriere 2001; Lepp, Stancil & Dalgarno 2002). The abundance in space of noble gases such as neon (one of the six most present components in our Solar system) (Asplund et al. 2009) is in a great amount (Yao & Wang 2006; Bochsler et al. 2012; Park et al. 2014). The presence of neon, which came from the Solar wind, has been recently shown in the lunar exosphere (Koner et al. 2016). In the last decade, cationic noble gas hydrides (NgH^+, Ng = He, Ne and Ar) have been the subject of various investigations both theoretically and experimentally (Milleur, Matcha & Hayes 1974; Rosenkrantz 1990; Fridgen & Parnis 1998). In fact, because of the abundance of their constituting elements (noble gas and proton) (Zygelman et al. 1998; Ferriere 2001; Grandinetti 2011), cationic noble gas hydrides play a crucial role in several cosmological phenomena (Zygelman et al. 1998; Lepp et al. 2002; Dalgarno 2006). These observations along with the highly investigated and approved mechanism of formation (see equation (1)) led us to expect the presence of NgH^+ in the interstellar and circumstellar media:

$$Ng + H_2^+ \longrightarrow NgH^+ + H. \quad (1)$$

Indeed, argonium (ArH^+) was observed in the Crab nebula (Barlow et al. 2013) towards diffuse clouds (Schilke et al. 2014) and more recently in the extragalactic space (Müller et al. 2015). Surprisingly, neonium (NeH^+) has not yet been detected despite it being essentially formed via the reaction mentioned above, and neon being more abundant in the interstellar medium (ISM) than argon (Theis & Fortenberry 2016). Both items predict that the interstellar neonium population should be close to that of argonium. In addition, NeH^+ may be detected in radio-astronomy since its electric dipole moment (∼3 D) (Rosmus & Reinsch 1980) is large enough and close to that of ArH^+ (Laughlin et al. 1989). Due to the high spatial and spectral resolutions of observatories such as the Atacama Large Millimeter Array (ALMA), the observation of neonium is expected. Hence, neonium formation has revived interest in various fields (in particular astrochemistry and plasma chemistry) and has been the subject of both theoretical and experimental reports. For example, time-dependent quantum dynamics, resonances in proton transfer, the effect of vibrational excitation, quantum statistical and quasi-classical trajectory, state-to-state dynamics, differential and integral cross-sections and dissociative recombination have been studied through the reaction mentioned above. Most of these

★ E-mail: cheikhtidiane.bop@ucad.edu.sn

findings have predicted the NeH^+ formation from $Ne + H_2^+$, where the H_2^+ reactant must be in an excited vibrational state ($\upsilon > 1$) (Moran & Friedman 1963).

Collisional as well as radiative rate coefficients are of great importance in modelling astrochemical environments (Roueff, Alekseyev & Le Bourlot 2014). Therefore, due to the lack of such studies on noble gas hydride ions, Barlow et al. (2013) used the data of the SiH^+ −He (Nkem et al. 2009) collisional system instead of those of the $ArH^+ - H_2$ complex to estimate the critical H_2 density. Our previous work on the ArH^+ −He (Bop et al. 2017) collisional system has shown that this approximation is not suitable since the potential energy surfaces of these complexes (ArH^+ −He and SiH^+ −He) differ by shape and well depth and different propensity rules were also observed. Without the collision rate coefficients, we are restricted to estimate the abundances of interstellar molecules using the approximation of local thermodynamic equilibrium that is not generally verified. Indeed, Hamilton et al., on ArH^+ excitation by electron impact, have calculated a $(2 \longrightarrow 1)/(1 \longrightarrow 0)$ line emission ratio of ∼31 which is significantly larger than the ratio of 2–2.5 observed in the Crab nebula (Barlow et al. 2013). They conclude that the observation suggests a non-local thermodynamic equilibrium excitation of ArH^+. From rotational spectral emission lines, the abundance of interstellar molecules may be accurately estimated depending on the accuracy of rate coefficients induced by collision with the most abundant gas (He or H_2) in the ISM.

These may be used as a template later, in particular the data obtained using He as a projectile, to approximate those worked out with para-H_2 ($j = 0$) as a collisional partner. In fact, helium may be used as a model for para-H_2 since it is a closed shell atom containing two electrons. The validity of this estimation for molecular hydrides is questionable (Lanza et al. 2014). However, good agreement has been found between the excitations of HCO^+ induced by para-H_2 (Flower 1999) and He (Monteiro 1985). Therefore, collisional processes of cationic molecular hydrides induced by helium are well studied despite the ambiguity mentioned above (Dubernet, Quintas-Sánchez & Tuckey 2015; Werfelli et al. 2017). It is obvious that molecular cationic hydrides strongly interact with H_2 and thus present very deep potential wells making the scattering processes computationally expensive. Nevertheless, the recorded data using He as collisional partner lead approximately to the cationic hydrides scattering processes in terms of magnitude rank. Monteiro (1985) has suggested, for charged species, to use a scale factor of 2–4 to derive rate coefficients induced by collision with para-H_2 from those obtained with He. To the best of our knowledge, rotational excitation of neonium induced by collision with helium has not yet been recorded despite its relevance for both chemical and astrophysical communities.

This paper is structured as follows: Section 2 presents the computational details, in Section 3 we discuss the results and the concluding remarks are given in Section 4.

2 COMPUTATIONAL DETAILS

2.1 Electronic calculations

The potential energy surface presented in this paper models the interactions between an atom and a rigid rotator diatomic molecule. Such calculations are often performed by keeping held the internuclear distance of the molecule fixed at its experimental equilibrium distance. For investigating excitation of the NeH^+ diatomic hydride by He, we have computed a three-dimensional potential energy surface (3D PES) instead of a pure two-dimensional potential energy surface (2D PES) as suggested by Kalugina, Lique & Marinakis (2014).

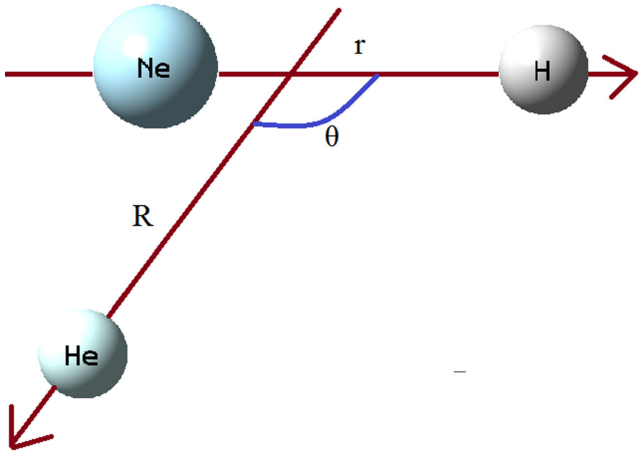

Figure 1. Body-fixed Jacobi coordinates system.

The NeH^+ −He complex may be described using the usual body-fixed Jacobi coordinates system r, R and θ, where r is the NeH^+ internuclear distance, R represents the distance between the centre of mass of the NeH^+ molecule and the helium atom and θ is the angle between the two distance vectors (see Fig. 1). The interaction potential was calculated by considering five values (1.43, 1.54, 1.85, 2.24 and 2.31 a_0) of the r-distance which led us to safely describe the three lowest vibrational levels of the molecule. In addition, the angular scattering coordinate θ was varied using a uniform step size of 10° from 0 to 180° and we considered 44 values for the radial coordinate (R = 2.50, 2.75, 3.00, 3.25, 3.50, 3.75, 4.00, 4.25, 4.50, 4.75, 5.00, 5.25, 5.50, 5.75, 6.00, 6.25, 6.50, 6.75, 7.00, 7.25, 7.50, 7.75, 8.00, 8.25, 8.50, 8.75, 9.00, 9.25, 9.50, 9.75, 10, 11, 12, 13, 14, 15, 16, 17, 18, 19, 20, 30, 50 and 100 a_0). Hence, the 3D potential energy surface was constructed with 4180 geometries treated in the C_s symmetry group. The calculations were performed using the explicitly correlated coupled cluster method with simple, double and perturbative triple excitation (CCSD(T)–F12) (Knizia, Adler & Werner 2009) in connection with the augmented–correlation consistent–polarized valence triple zeta (aug–cc–pVTZ) Gaussian basis set (Dunning Jr 1989; Kendall, Dunning & Harrison 1992) as implemented in the MOLPRO molecular package (Werner et al. 2009). A preliminary check was carried out using CASSCF computations. For the 4180 geometries mentioned above, the dominant configuration of the ground state has a weight of about 0.98. This has led us to use the monoconfigurational standard coupled cluster method. For explicitly correlated investigations, we follow the methodology established by Lique, Kłos & Hochlaf (2010). Because of the inclusion of triple perturbative excitations, the CCSD(T)–F12 method is not size consistent. This error has been corrected by shifting the global potential using the value obtained at 100 a_0 which is almost equal to 5 cm^{-1} and thus the potential is forced to asymptotically decay to zero. The basis set superposition error has also been corrected using the counterpoise procedure of Boys & Bernardi (1970):

$$V(r, R, \theta) = E_{NeH^+-He}(r, R, \theta) - E_{NeH^+}(R, \theta) - E_{He}(r, R, \theta). \quad (2)$$

The level of theory used in this work (CCSD(T)–F12/aug–cc–pVTZ) is well studied in the literature (Ajili et al. 2016; Bouhafs et al. 2017). However, we present in Table 1 some ab initio

Table 1. Interaction potential (in units of cm^{-1}) of the NeH$^+$ −He complex for three arrangements ($\theta = 0°$, 90° and 180°) as a function of the scattering R-distance (a_0) computed at different levels of theory. The neonium internuclear distance is held fixed at the experimental value $r_{\rm NeH^+} = r_{\rm e} = 1.85\ a_0$.

	0°			90°			180°		
R	CCSD(T)/aV5Z	CCSD(T)–F12/aVTZ	CCSD(T)/CBS	CCSD(T)/aV5Z	CCSD(T)–F12/aVTZ	CCSD(T)/CBS	CCSD(T)/aV5Z	CCSD(T)–F12/aVTZ	CCSD(T)/CBS
3.00	10336.193	10350.532	10292.010	6205.490	6211.453	6191.922	6497.803	6507.253	6488.855
3.25	1062.571	1064.188	1033.690	3108.420	3110.130	3097.862	3266.227	3271.741	3258.677
3.50	− 2302.732	− 2305.978	− 2323.149	1433.334	1432.648	1425.008	1537.453	1540.107	1531.353
3.75	− 3195.013	− 3198.840	− 3210.562	552.576	550.359	545.913	636.660	637.267	631.927
4.00	− 3088.698	− 3091.689	− 3099.538	108.892	105.491	103.364	184.781	183.835	181.072
4.25	− 2636.266	− 2638.418	− 2643.362	− 99.211	− 103.344	− 103.826	− 28.656	− 30.577	− 31.569
4.50	− 2120.990	− 2122.328	− 2126.407	− 183.868	− 188.293	− 187.761	− 118.758	− 121.130	− 121.130
4.75	− 1655.065	− 1655.525	− 1658.963	− 206.480	− 210.829	− 209.936	− 147.437	− 149.869	− 149.491
5.00	− 1272.332	− 1272.132	− 1275.015	− 199.939	− 203.950	− 203.044	− 147.303	− 149.548	− 149.160
5.25	− 973.064	− 972.482	− 974.941	− 181.353	− 184.889	− 184.164	− 135.057	− 137.034	− 136.809
5.50	− 745.198	− 744.492	− 746.532	− 159.258	− 162.258	− 161.680	− 118.923	− 120.643	− 120.474

points of the NeH$^+$ −He potential computed at different levels of theory. In these calculations, the neonium internuclear distance was frozen at the experimental equilibrium value $r_{\rm NeH^+} = r_{\rm e} = 1.85\ a_0$ (Ram, Bernath & Brault 1985). For the standard coupled cluster method, the Ne, H and He atoms were described by the aug–cc–pVXZ (X = D, T and Q) basis sets (Dunning Jr 1989; Kendall et al. 1992). In addition, bond functions ($3s3p2d2f1g$) defined by Cybulski & Toczyłowski (1999) were placed at mid-distance between the centre of mass of the NeH$^+$ molecule and the He atom. It was then possible to extrapolate the ab initio interaction potential to the Complete Basis Set (CBS) limit, using the Gaussian formula (Peterson, Woon & Dunning 1994; Feller & Sordo 2000) and the mixed exponential:

$$E_{\rm X} = E_{\rm CBS} + A{\rm e}^{-(X-1)} + B{\rm e}^{-(X-1)^2}, \tag{3}$$

where $E_{\rm CBS}$, A and B are adjustable parameters and $X = 2$, 3 and 4. The CCSD(T)/aug–cc–pV5Z and the CCSD(T)–F12/aug–cc–pVTZ methods lead to similar data to the values obtained using the CCSD(T)/CBS approach. In fact, compared to the CCSD(T)/CBS data, both CCSD(T)–F12/aug–cc–pVTZ and CCSD(T)/aug–cc–pV5Z present relative errors less than 3 per cent for all considered ab initio points, confirming the accuracy of the level of theory used in this paper.

2.2 Scattering calculations

Integral state-to-state inelastic cross-sections were computed with the CC method of Arthurs & Dalgarno (1960) implemented in the MOLSCAT program for total energies (E) up to 4000 cm^{-1}. The dynamic calculations were performed using the Manolopoulos (1986) propagator to solve the coupled differential equations. It is noteworthy that this is required to define the parameters of the propagator. The integration limits of the scattering calculations were set to $R_{\rm min} = 2a_0$ and $R_{\rm max} = 90a_0$. The STEPS-parameter along with the kinetic energy ($E_{\rm c}$) are inversely proportional to the step of integration. Therefore, the STEPS-parameter is set to 20 for $E < 100$ cm^{-1} and to 10 for $E \geq 100$ cm^{-1}. All these propagator parameters were adjusted by performing convergence tests as it is usually done (Al Mogren et al. 2015; Hernández Vera et al. 2017). In addition, the rotational basis was optimized in order to include into dynamic calculations all opened channels along with enough closed channels: for $E < 1000$ cm^{-1} the number of closed channels were set to 10, 7 for $1000 \leq E < 2000$ cm^{-1} and up to 6 for $E = 4000$ cm^{-1}. The rotational energies ($E_{\rm J}$) of the NeH$^+$ molecule were obtained with the usual expansion depending on the experimental rotational ($B_{\rm e} = 17.15846$ cm^{-1}) and centrifugal distortion ($D_{\rm e} = 2.4986 \times 10^{-3}$ cm^{-1}) constants of Ram et al. (1985). By attributing to the diagonal and off-diagonal tolerances values of 0.01 and 0.001 Å^2, respectively, the convergence of inelastic cross-sections is ensured with 0.1 per cent error leading to achieve large value of total angular momentum ($J_{\rm tot}$). For example, we have recorded $J_{\rm tot} = 160$ at 100 cm^{-1}, 296 at 1000 cm^{-1}, 314 for $E = 2000$ cm^{-1} and 335 for $E = 4000$ cm^{-1}. The rotational cross-sections were computed by carefully spanning the grid of energy: for $E < 100$ cm^{-1} the step was set to 0.1 cm^{-1}, for $100 \leq E < 150$ cm^{-1} to 0.2 cm^{-1}, for $150 \leq E < 200$ cm^{-1} to 0.5 cm^{-1}, for $200 \leq E < 300$ cm^{-1} to 1 cm^{-1}, for $300 \leq E < 500$ cm^{-1} to 5 cm^{-1}, for $500 \leq E < 1000$ cm^{-1} to 10 cm^{-1}, for $1000 \leq E < 2000$ cm^{-1} to 20 cm^{-1}, for $2000 \leq E < 3000$ cm^{-1} to 50 cm^{-1} and for $3000 \leq E < 4000$ cm^{-1} to 100 cm^{-1}.

By thermally averaging these cross-sections using the velocity distribution of Maxwell–Boltzmann, we have computed the collision rate coefficients for kinetic temperatures ranging from 4 to 300 K.

$$\tau_{J \longrightarrow J'}(T) = \left(\frac{8\beta^3}{\pi\mu}\right)^{1/2} \int_0^\infty E_{\rm c}\sigma(E_{\rm c}){\rm e}^{-\beta E_{\rm c}}{\rm d}E_{\rm c}, \tag{4}$$

$\beta = 1/k_{\rm B}T$, where $k_{\rm B}$ represents the constant of Boltzmann, T is the kinetic temperature, the kinetic energy $E_{\rm c}$ is obtained by subtracting the rotational energy ($E_{\rm J}$) from the total energy (E) and $\mu = 3.36$ au is the reduced mass of the collisional system. The downward collision rates were carried out for rotational transitions involving the 11 first levels.

3 RESULTS AND DISCUSSIONS

3.1 Interaction potential and analytical fit

The calculated ab initio 3D PES was averaged over the fundamental vibrational level ($\varphi_{\upsilon=0}$) of the NeH$^+$ molecule. The fitting procedure described by Werner, Follmeg & Alexander (1988) for the CN−He system was adopted in order to obtain the $V(r, R, \theta)$ numerical expansion routine required to perform the dynamical calculations. The potential was fitted to the functional form:

$$V(r, R, \theta) = \sum_{n=1}^{N}\sum_{l=1}^{L} A_{\rm ln}(R){\rm d}_{m,0}^{l+m-1}(\cos\theta)(r - r_{\rm e})^{n-1}, \tag{5}$$

where the ${\rm d}_{m,0}^{l+m-1}$ are the reduced Wigner rotation matrix elements, N and L represent the numbers of the NeH$^+$ molecule internuclear distances and the scattering angles considered in the 3D–PES determination, respectively. The average PES ($V_{\upsilon,\upsilon'}$) was then obtained using the following algorithm:

$$V(R, \theta) = < \varphi_{\upsilon=0}(r) \mid V(r, R, \theta) \mid \varphi_{\upsilon'=0}(r) >, \tag{6}$$

Table 2. Matrix elements computed in this work, the $M_{0,0}(n)$ components were used in the averaging of the 3D–PES.

n	$M_{0,0}(n)$	$M_{0,1}(n)$	$M_{0,2}(n)$	$M_{1,1}(n)$	$M_{1,2}(n)$	$M_{2,2}(n)$
1	1.000	0.000	0.000	1.000	0.000	1.000
2	0.047	0.149	0.022	0.146	− 0.215	0.254
3	0.025	0.023	− 0.027	0.091	− 0.071	0.187
4	0.004	0.013	− 0.008	0.030	− 0.050	0.096
5	0.002	0.004	− 0.006	0.016	− 0.025	0.064

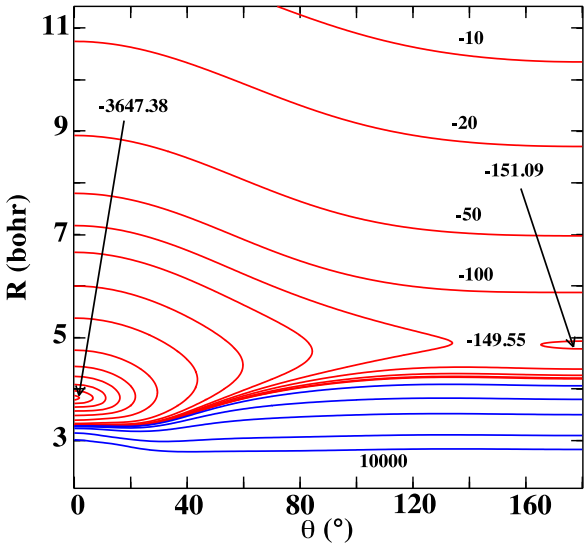

Figure 2. Contour plot of the NeH^+ ($X^1\Sigma^+$)–$He(^1S)$ PES (in units of cm^{-1}) as a function of R and θ. The zero of energy corresponds to the NeH^+–He asymptote.

taking into account equation (5), we have:

$$V(R,\theta) = \sum_{n=1}^{N}\sum_{l=1}^{L} A_{\ln}(R)\mathrm{d}^{l+m-1}_{m,0}(\cos\theta) \times M_{0,0}(n),$$

$$M_{\upsilon,\upsilon'}(n) = < \varphi_{\upsilon}(r) \mid (r - r_e)^{n-1} \mid \varphi_{\upsilon'}(r) > \qquad (7)$$

The vibrational wave functions were obtained by the Fourier Grid Hamiltonian method (Marston & Balint-Kurti 1989; Balint-Kurti, Dixon & Marston 1992) from the NeH^+ potential computed at the CCSD(T)-F12/aug–cc–pVTZ level of theory. The most relevant matrix elements $M_{\upsilon,\upsilon'}(n)$ are given in Table 2.

Fig. 2 depicts the contour plot of the average NeH^+ −He PES as a function of R and θ. The blue lines correspond to positive energy values and red contours are for negative energies. This interaction PES shows two potential wells of 3647.38 and 151.09 cm^{-1} located at (R, θ) = (3.75 a_0, 0°) and (4.75 a_0, 180°) corresponding to the linear geometries NeH^+···He and He···NeH^+, respectively. A transition state occurs at 149.55 cm^{-1} between the $NeHHe^+$ and $HeNeH^+$ isomers at the coordinates (R, θ) = (5.00 a_0, 150°). One can conclude that the anisotropy of the PES is particularly observed for θ = 0–150° contrary to the ArH^+ −He PES. Both collisional systems present two global minima at the linear He orientations; however, the well observed at 0° (180°) is deeper (less deep) for NeH^+ −He than for ArH^+ −He. The difference in behaviour of these interaction potentials may be explained by calculating the charge repartition over the atoms of the two molecules NeH^+ and ArH^+. For neonium, the positive charge is shifted to H at 80 per cent while for argonium it is distributed at almost equal proportions

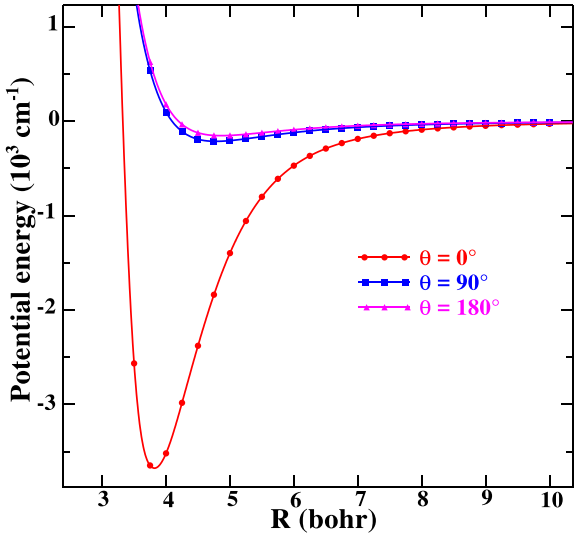

Figure 3. Cuts of the average interaction potential as a function of the scattering R-distance for three angle values θ = 0°, 90° and 180°

(52 per cent for H and 48 per cent for Ar). These data are obtained from the Mulliken population analysis at the CCSD(T)–F12/aug–cc–pVTZ level of theory.

For a better appreciation of the variation of the anisotropy, we present in Fig. 3 three cuts of the average interaction potential which are $V(R_{NeH^+\cdots He},\ \theta = 0°)$, $V(R_{NeH^+\perp He},\ \theta = 90°)$ and $V(R_{He\cdots NeH^+},\ \theta = 180°)$: $R_{NeH^+\cdots He}$ is the scattering R-distance for He approach towards H, $R_{He\cdots NeH^+}$ for He approach towards Ne and $R_{NeH^+\perp He}$ represents R in the T-shape geometry. As mentioned above, at the linear He orientations θ = 0° and 180°, the potential wells are 3647.38 and 151.09 cm^{-1} and occur at 3.75 and 4.75 a_0, respectively. These well depths are very different leading to a strong anisotropy of the potential between 0 and 180°. The minimum (206.15 cm^{-1}) occurs at R = 5 a_0 in the T-shape geometry. This energy value is close to the potential well observed at 180° reducing considerably the anisotropy from 90°.

In order to perform scattering calculations, we have fitted the average potential on the basis of Legendre polynomial functions to enable the basic input required by the MOLSCAT program:

$$V(R,\theta) = \sum_{\lambda=0}^{\lambda_{max}} V_\lambda(R) P_\lambda(\cos\theta). \qquad (8)$$

From the average interaction potential calculated for 19 scattering angles (which correspond to 19 values of λ), we include terms up to λ_{max} = 18 in the expansion. Fig. 4 displays the expansion of the four first V_λ radial coefficients as a function of R. With respect to the anisotropic radial coefficients (terms for which λ > 0), the largest in magnitude is V_1.

3.2 Cross-sections and rate coefficients

Fig. 5 presents the rotational excitation cross-sections of NeH^+ induced by collision with He as a function of the kinetic energy for 0 ⟶ J (upper panel) and ΔJ = 1 (lower panel) transitions. The cross-sections increase quickly up to a threshold value and decrease progressively to an asymptotic value. Several resonances are observed for energies below 500 cm^{-1}. This behaviour was notified in early works (Smith, Malik & Secrest 1979; Christoffel & Bowman 1983) as well as in the recent ones (Kalugina et al. 2014;

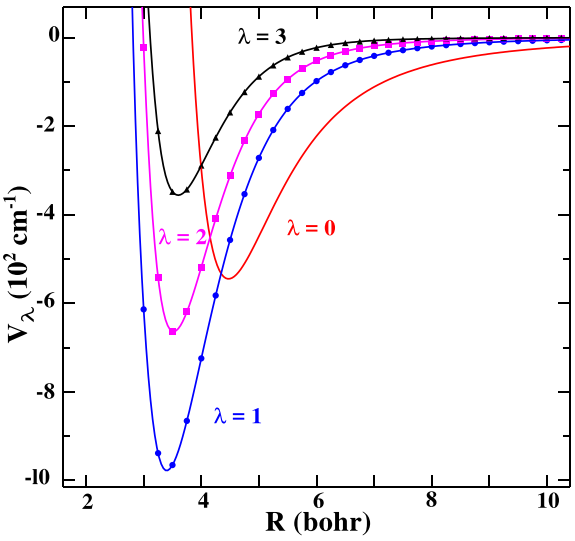

Figure 4. Expansion of the four first radial coefficients $V_{\lambda=0-3}$ as a function of R.

Bop et al. 2017). It was interpreted as temporary trapping of helium around the potential well, where the complex (NeH$^+$–He) forms quasi-bound states. It is noteworthy to remind that at low energy a fine grid was used and for higher energy values the step size was carefully increased. This procedure is of great interest for a correct description of the resonances. Concerning propensity rules, the 0 ⟶ 1 transition absolutely predominates in the two panels. In the lower panel, an inversion is observed from 300 to 1000 cm^{-1} between the 3 ⟶ 4 and 4 ⟶ 5 transitions. A similar behaviour was noted between the 0 ⟶ 1 and 1 ⟶ 2 transitions for ArH$^+$–He collisional system. From the analysis of these curves, one can conclude that transitions involving odd ΔJ values outweigh the even ones. This propensity rule in favour of odd transitions emanates from the predominance of the anisotropic V_1 term (see Fig. 4) and is expected to persist for the collisional rates.

We present in Fig. 6 rate coefficients of NeH$^+$ induced by collision with He as a function of kinetic temperature for $J \longrightarrow 0$ (upper panel) and $\Delta J = 1$ (lower panel) transitions. It is clear from the upper panel that the $1 \longrightarrow 0$ transition strongly outweighs and thus confirming the propensity rules mentioned above. Propensity rules in favour of odd transitions were also observed in the work of Hamilton, Faure & Tennyson (2016) for HeH$^+$ and ArH$^+$ excited by electron impact. The lower panel where we depict curves of dominant transitions (i.e. transitions involving odd ΔJ values) shows that the 3 ⟶ 2, 5 ⟶ 4 and 2 ⟶ 1 rotational transitions predominate almost in the entire kinetic temperature range. This behaviour has let us predict that these transitions are the most probable rotation emission lines to detect the NeH$^+$ ion. Laboratory experiments, carried out at low temperature ($T < 50$ K) such as in Hauser et al. (2015), should detect the 3 ⟶ 2 and 5 ⟶ 4 transitions. The 3 ⟶ 2 and 5 ⟶ 4 downward rate coefficients which are predominant in the temperature range of 50–300 K could be detected in diffuse clouds and also in hot environments such as the Crab nebula. It is noteworthy to remind that the ArH$^+$ 2 ⟶ 1 and 1 ⟶ 0 transitions, which are in the same magnitude rank (2.40–2.91 $\times$ 10^{-10} and 0.88–1.20 $\times$ 10^{-10} cm^3 s^{-1}, respectively) as the above transitions, were observed in the Crab nebula (Barlow et al. 2013) and in diffuse clouds (Schilke et al. 2014). In addition, observatories with high spectral and special resolutions such as the ALMA may record the 2 ⟶ 1 and 4 ⟶ 3 rotational emission lines.

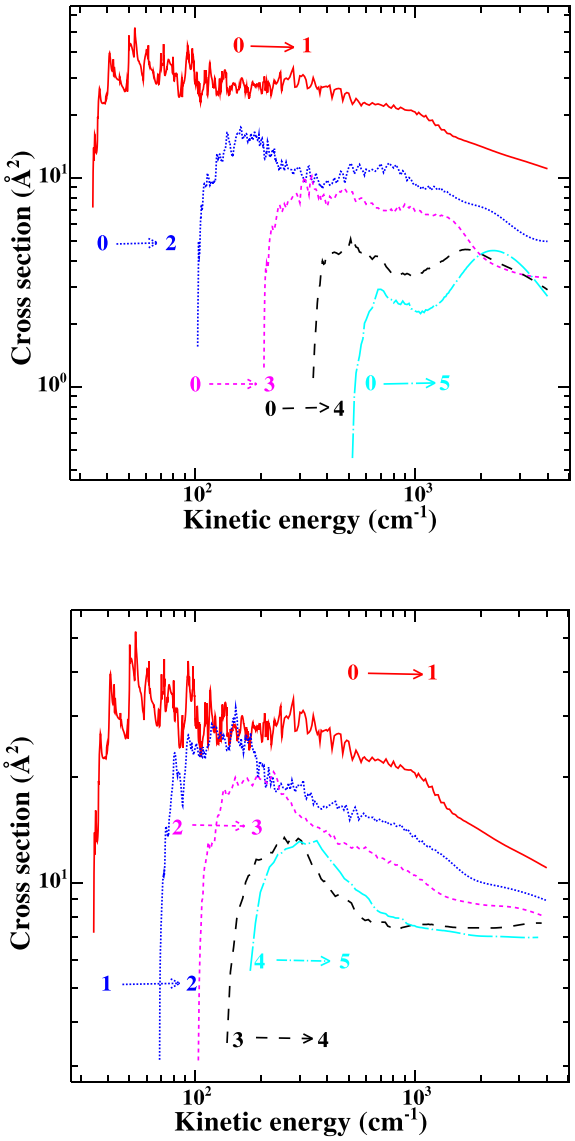

Figure 5. Integral inelastic cross-sections of NeH$^+$ induced by collision with He as a function of the kinetic energy for 0 ⟶ J (upper panel) and $\Delta J = 1$ (lower panel) transitions.

4 CONCLUSION

Rotational integral inelastic cross-sections of neonium induced by collision with helium have been calculated using the CC quantum mechanical approach for energies ranging from 34.4 to 4000 cm^{-1}. These data have been thermally averaged over the Maxwell–Boltzmann velocity distribution leading to determine rate coefficients among the 11 first rotational levels in the kinetic temperature range of 3–300 K. These scattering calculations were performed on an average interaction potential. This latter was obtained from a new 3D potential energy surface computed with the explicitly correlated coupled cluster with single, double and perturbative triple excitation in connection with the aug–cc–pVTZ Gaussian basis set.

In this paper, we note that propensity rules for cross-sections as well as downward rate coefficients are in favour of odd ΔJ transitions. This is in agreement with propensities observed for HeH$^+$ and ArH$^+$ (Hamilton et al. 2016; Bop et al. 2017). For the 2 ⟶ 1 transition, the average ratio over the temperature grid (4–300 K) of downward rate coefficients NeH$^+$/ArH$^+$ (∼0.83) is

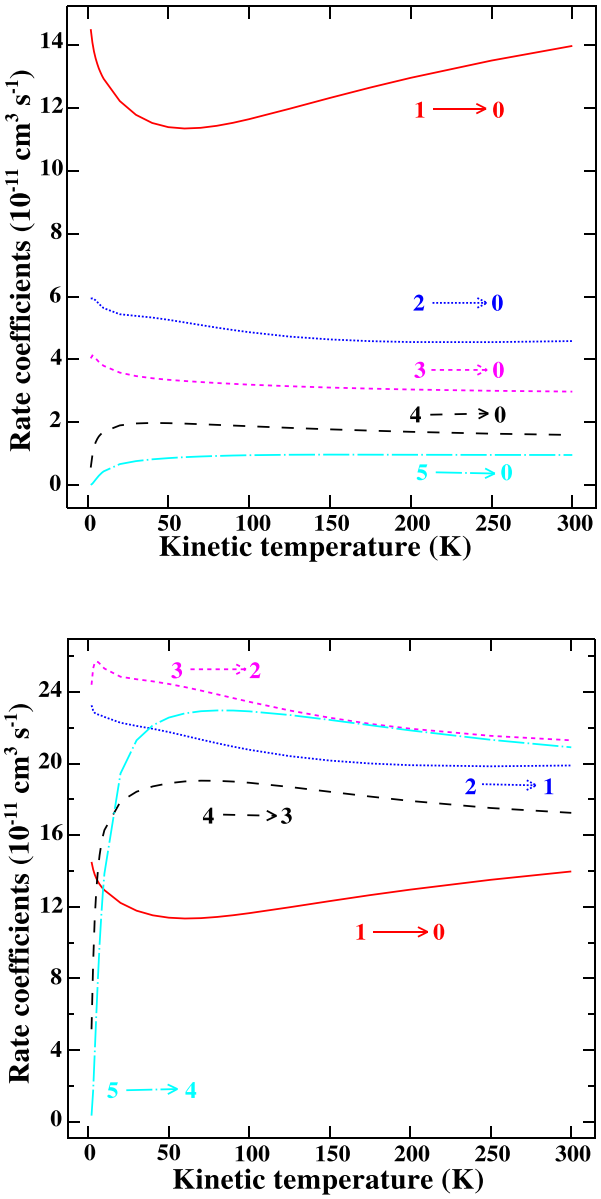

Figure 6. Rotational rate coefficients of NeH^+ induced by collision with He as a function of the kinetic temperature for $J \longrightarrow 0$ (upper panel) and $\Delta J = 1$ (lower panel) transitions.

close to unity. It is relevant to mention that this transition is dominant for ArH^+ and appears at the third rank for NeH^+ after $3 \longrightarrow 2$ and $5 \longrightarrow 4$. This confirms that the key neonium may be present in interstellar and circumstellar media since rotational emission line intensities of argonium corresponding to the $2 \longrightarrow 1$ transition were recorded in several astrophysical environments (Barlow et al. 2013; Schilke et al. 2014; Müller et al. 2015). The data computed in this paper may be crucial for the eventual investigations focused to detect the key neonium in the interstellar and circumstellar media as well as in laboratory experiments.

ACKNOWLEDGEMENTS

This work is supported by the Abdus Salam International Centre for Theoretical Physics, Office of External Activities (ICTP-OEA) under NET45 program.

REFERENCES

Ajili Y., Abdallah D. B., Al-Mogren M. M., Francisco J., Hochlaf M., 2016, MNRAS, 458, 1581
Al Mogren M. M., Ajili Y., Almania S., Abdallah D. B., Hochlaf M., 2015, MNRAS, 452, 1561
Arthurs A., Dalgarno A., 1960, Proc. R. Soc., 256, 540
Asplund M., Grevesse N., Sauval A. J., Scott P., 2009, ARA&A, 47, 481
Balint-Kurti G. G., Dixon R. N., Marston C. C., 1992, Int. Rev. Phys. Chem., 11, 317
Barlow M. et al., 2013, Science, 342, 1343
Bochsler P. et al., 2012, ApJS, 198, 13
Bop C. T., Hammami K., Niane A., Faye N., Jaïdane N., 2017, MNRAS, 465, 1137
Bouhafs N., Lique F., Faure A., Bacmann A., Li J., Guo H., 2017, J. Chem. Phys., 146, 064309
Boys S. F., Bernardi F., 1970, Mol. Phys., 19, 553
Christoffel K. M., Bowman J. M., 1983, J. Chem. Phy., 78, 3952
Cybulski S. M., Toczyłowski R. R., 1999, J. Chem. Phys., 111, 10520
Dalgarno A., 2006, Faraday Discuss., 133, 9
Dubernet M.-L., Quintas-Sánchez E., Tuckey P., 2015, J. Chem. Phys., 143, 044315
Dunning T. H., Jr, 1989, J. Chem. Phys., 90, 1007
Feller D., Sordo J. A., 2000, J. Chem. Phys., 112, 5604
Ferriere K. M., 2001, Rev. Mod. Phys., 73, 1031
Flower D., 1999, MNRAS, 305, 651
Fridgen T. D., Parnis J. M., 1998, J. Chem. Phys., 109, 2162
Grandinetti F., 2011, Eur. J. Mass Spectrom., 17, 423
Hamilton J. R., Faure A., Tennyson J., 2016, MNRAS, 455, 3281
Hauser D. et al., 2015, Nature Phys., 11, 467
Hernández Vera M., Lique F., Dumouchel F., Hily-Blant P., Faure A., 2017, MNRAS, 468, 1084
Kalugina Y., Lique F., Marinakis S., 2014, Phys. Chem. Chem. Phys., 16, 13500
Kendall R. A., Dunning T. H., Jr, Harrison R. J., 1992, J. Chem. Phys., 96, 6796
Knizia G., Adler T. B., Werner H.-J., 2009, J. Chem. Phys., 130, 054104
Koner D., Barrios L., González-Lezana T., Panda A. N., 2016, J. Chem. Phys., 144, 034303
Lanza M., Kalugina Y., Wiesenfeld L., Faure A., Lique F., 2014, MNRAS, 443, 3351
Laughlin K., Blake G. A., Cohen R., Saykally R., 1989, J. Chem. Phys., 90, 1358
Lepp S., Stancil P., Dalgarno A., 2002, J. Phys. B: At. Mol. Opt. Phys., 35, R57
Lique F., Kłos J., Hochlaf M., 2010, Phys. Chem. Chem. Phys., 12, 15672
Manolopoulos D., 1986, J. Chem. Phys., 85, 6425
Marston C. C., Balint-Kurti G. G., 1989, J. Chem. Phys., 91, 3571
Milleur M. B., Matcha R. L., Hayes E. F., 1974, J. Chem. Phys., 60, 674
Monteiro T., 1985, MNRAS, 214, 419
Moran T., Friedman L., 1963, J. Chem. Phys., 39, 2491
Müller H. S. et al., 2015, A&A, 582, L4
Nkem C., Hammami K., Manga A., Owono L. O., Jaidane N., Lakhdar Z. B., 2009, J Mol. Struct.: THEOCHEM, 901, 220
Park J. et al., 2014, ApJ, 795, 97
Peterson K. A., Woon D. E., Dunning T. H., Jr, 1994, J. Chem. Phys., 100, 7410
Ram R., Bernath P., Brault J., 1985, J. Mol. Spectrosc., 113, 451
Rosenkrantz M. E., 1990, Chem. Phys. Lett., 173, 378
Rosmus P., Reinsch E.-A., 1980, Z. Nat. A, 35, 1066
Roueff E., Alekseyev A., Le Bourlot J., 2014, A&A, 566, A30
Schilke P. et al., 2014, A&A, 566, A29
Smith L. N., Malik D. J., Secrest D., 1979, J. Chem. Phys., 71, 4502
Theis R. A., Fortenberry R. C., 2016, Mol. Astrophys., 2, 18
Werfelli G., Balança C., Stoecklin T., Kerkeni B., Feautrier N., 2017, MNRAS, 468, 2582
Werner H.-J., Follmeg B., Alexander M. H., 1988, J. Chem. Phys., 89, 3139
Werner H.-J. et al., 2009, A&A, 47, 481

Yao Y., Wang Q. D., 2006, ApJ, 641, 930
Zygelman B., Stancil P., Dalgarno A., 1998, ApJ, 508, 151

SUPPORTING INFORMATION

Supplementary data are available at *MNRAS* online.

rate-tab.pdf

Please note: Oxford University Press is not responsible for the content or functionality of any supporting materials supplied by the authors. Any queries (other than missing material) should be directed to the corresponding author for the article.

This paper has been typeset from a TEX/LATEX file prepared by the author.